**Please cite the Published Version**

Kulczyk-Malecka, J, Santos, IVJD, Betbeder, M, Rowley-Neale, SJ, Gao, Z and Kelly, PJ (2021) Low-temperature synthesis of vertically aligned graphene through microwave-assisted chemical vapour deposition. Thin Solid Films, 733. p. 138801. ISSN 0040-6090

**DOI:** https://doi.org/10.1016/j.tsf.2021.138801

**Publisher:** Elsevier

**Version:** Accepted Version

**Additional Information:** This is an Author Accepted Manuscript of an article published in Thin Solid Films.

# Low-temperature synthesis of vertically aligned graphene through microwave-assisted chemical vapour deposition

Justyna Kulczyk-Malecka[1*†], Isabella V. J. dos Santos[1†], Marine Betbeder[1], Samuel Rowley-Neale[2], Zhaohe Gao[3], Peter J. Kelly[1]

[1]*Surface Engineering Group, Manchester Fuel Cell Innovation Centre, Manchester Metropolitan University, Manchester M1 5GD, UK*

[2]*Faculty of Science and Engineering, Manchester Fuel Cell Innovation Centre, Manchester Metropolitan University, Manchester M1 5GD, UK*

[3]*Henry Royce Institute, Department of Materials, University of Manchester, Manchester, M13 9PL, UK*

[†] Co-Authors: These authors contributed equally to this work.

*Corresponding author. Tel: 0044 161 247 1201. Email: j.kulczyk-malecka@mmu.ac.uk
(Justyna Kulczyk-Malecka)

**Abstract:** The intrinsic properties of vertically aligned graphene (VG), such as high ratio of exposed active edges compared to inert basal sites, non-stacking morphology and large surface-to-volume ratio make it applicable to numerous advanced technologies such as sensors, flexible electronics and fuel cells. Plasma-enhanced chemical vapour deposition (PECVD) has emerged as a promising technique to synthesise graphene at lower temperatures than a conventional chemical vapour deposition (CVD) process, providing a better control over the deposition parameters to tailor graphene properties.

This study presents a cost effective, scalable, single step synthesis of a high quality VG at low temperatures. The samples were synthesised in a microwave (MW) assisted CVD reactor, allowing for decomposition of $CH_4$ and $H_2$ gas mixtures in Ar as a carrier gas, and VG growth directly onto Si wafer substrates without an additional heat applied to the substrate. Deposition conditions, such as MW power, gas ratio, and substrate-to-plasma separation were optimized to tailor the morphology, growth rate and electrochemical performance of the VG. The physiochemical analysis revealed that the fabricated VG consisted of high quality vertically aligned $sp^2$ graphene, whilst a cyclic voltammetry (CV) analysis confirmed that the structures are electrochemically active and demonstrate a typical characteristics of quasi-reversible processes.

**Key words:** Vertically aligned graphene, Microwave assisted chemical vapour deposition, Low temperature synthesis, Raman spectroscopy, X-ray photoelectron spectroscopy

## 1. Introduction

The fabrication and utilisation of vertically aligned graphene (VG) become a prevalent research topic due to the high conductivity of VG (resulting from its high number of exposed active edge sites), large surface area and excellent chemical stability. An increased interest in the synthesis of free-standing graphene structures is related to the amount of defects and ordering in graphene based materials [1-5]. Vertically aligned graphene, also known as carbon nanowalls or vertically oriented graphene, consists of multilayer graphene sheets arranged perpendicular to the substrate, forming a mesh-like network. This unique branching shape allows the well-known properties of graphene (such as high electron mobility [6], thermal properties [7] and high strength [8]) to be combined with additional features that arise from the vertical orientation, such as the exposed reactive edges, improved mechanical stability and large surface area.

The controlled growth of VG leads to a porous three-dimensional structure of graphene, resulting in an extremely high surface area [9]. This in turn benefits applications relying on the storage of energy through charge accumulation at the electrode/electrolyte interface, such as supercapacitors [10] and batteries [11]. The vertically oriented graphene films also present abundant exposed edges. As presented by Brownson et al. [12], graphitic surfaces are heterogeneous in nature, with different electrochemical activity in the basal and edge planes. The latter has shown faster electrochemical reactions compared to the basal plane [13]. Thus, the open and exposed edge structures observed in VG are particularly important for applications depending on the edge activity (i.e. sensing [14] and fuel cells [15-17]). Moreover, graphene nanowalls are typically synthesised by plasma-enhanced chemical vapour deposition (PECVD) processes [1], which are a potential route to producing graphene materials at relatively low temperatures and on a large scale.

PECVD has recently emerged in the synthesis of graphene as an alternative to thermal chemical vapour deposition (CVD) [18], which is widely employed in the synthesis of high-quality monolayer graphene [19]. Even though CVD-graphene has shown promising properties [20, 21], the process itself is limited to catalytic substrates (i.e. Cu and Ni) and the synthesis occurs at high temperatures (1000ºC). PECVD has been used in the synthesis of carbon-related thin films, such as diamond-like carbon coatings [22, 23]. During the process, a glow-discharge plasma is sustained in a chamber where vapour-phase chemical reactions and film deposition occur. The plasma promotes the decomposition of carbon precursors such as $CH_4$ or $C_2H_2$ into active species (i.e. atoms, ions, radicals) by electron impact dissociation and ion bombardment. These events promote deposition at much lower temperature and higher rates when compared to conventional CVD [24]. Therefore, the growth is catalyst-free and the synthesis of graphene on temperature-sensitive substrates is feasible [25, 26]. Furthermore, another important advantage of the PECVD process is the excellent control over ordering/patterning nanostructures [27], which makes it possible to tune the physical properties of graphene, such as spatial orientation and density, to meet specific applications [1, 28-30]. The growth mechanism of VG is attributed to large concentrations of defects on the substrate surface due to plasma bombardment, which serve as nucleation sites for graphitic films to grow. It has been hypothesised that the VG rises from the curved area, i.e. defects or mismatches created by the plasma, which serve as active sites for VG nucleation and growth, resulting in graphene layers growing in the tangential direction. Open graphene edges formed at the top are also active sites onto which following carbon atoms attach, supplied as a result of diffusion of carbon adatoms on the surface of VG [5]. There are many benefits of the plasma environment affecting the growth of graphene, such as the ability to focus energetic ions on the substrate surface, creating a chemical potential gradient allowing for fast precursor delivery and film growth. Moreover, plasma increases the synthesis temperature and creates the electric-field induced polarization of the substrate surface, which reduces the bonding energy of atoms to the substrate surface and increases the diffusion coefficient, all of which facilitate film growth [5]. The presence of Ar carrier gas allows for plasma ionisation by providing high-energy electrons and helps the formation of $C_2$ species, which increase the degree of graphitisation on the substrate. High-energy species drive reactions, such as methane decomposition or molecular hydrogen dissociation and formation of reactive radicals without the need for applied heat (other than that created in the plasma bulk) [31]. In the work of Vishwakarma et al. VG growth mechanism in the presence of a MW plasma was attributed to the catalytic activity of hydrogen, which enables $C_nH_y$ species formation in the hot region of the plasma, as a result of the H-shifting reaction [32]. These energetic species (i.e. positive ions, radicals) are accelerated towards the grounded substrate, where the VG structures are grown. Due to the complexity of the process and the diversity of plasma sources used in the deposition of VG (such as RF [33], inductively coupled plasma (ICP) [4] and MW [34-37]) there are still controversial results reported in the literature and remaining challenges in standardising the growth of carbon nanowalls. Nevertheless, several authors have reported synthesis of VG at temperatures significantly lower (i.e. ~300 – 600ºC) than that of conventional CVD processes [18, 25, 32, 35, 38-42]. Herein the synthesis of vertical oriented graphene by microwave-assisted chemical vapour deposition (MW-CVD) is presented. VG samples were produced in a bespoke rector directly on non-catalytic Si wafer substrates and the process was carried out without additional heating or bias applied to the substrates, resulting in relatively low substrate temperatures (≤ 300 °C). The versatile process developed in this study proves that it is possible to tailor VG properties by adjusting the growth conditions, such as the plasma to substrate distance and deposition time. Therefore, this study contributes to the development and standardization of VG synthesis, aiming to advance the research of vertically oriented graphene nanosheets at a relatively low temperature range, allowing the use of temperature sensitive substrates and, in turn, expanding their potential applications.

## 2. Experimental

### *2.1 Chemicals and materials*

The chemicals used in this work were of analytical grade and used as received from the supplier Sigma-Andrich UK, this includes a solution of 1 mM $[Ru(NH_3)_6]^{3+/2+}$ and 0.1 M KCl and Ag/AgCl reference electrode .The coiled Pt wire counter electrode was purchased from Alvatek Ltd.

### *2.2 Synthesis of vertically aligned graphene*

VG was synthesised in a bespoke reactor equipped with a microwave power supply (MKS Instruments Ltd.) having a maximum power output of 3.0 kW at 2.45 GHz frequency. Fig. 1 schematic illustrates the MW-CVD reactor used in this study.

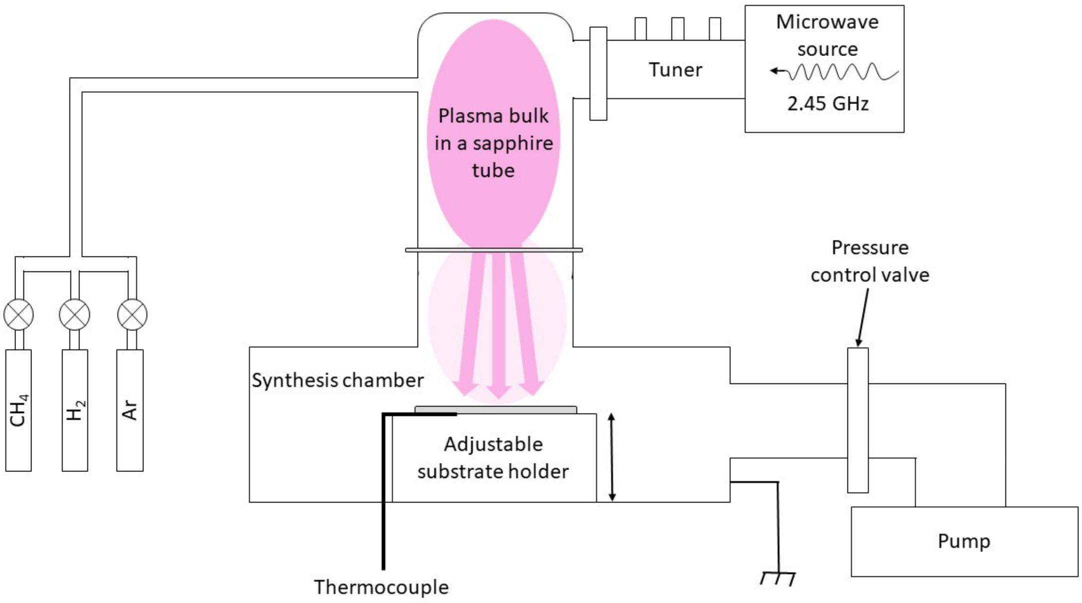

Prior to VG deposition, the chamber was pumped down to a base pressure of approximately 6.67x$10^{-3}$ Pa. A UV light source was used to facilitate ignition of the plasma discharge and provide stability during the synthesis. The pressure during the deposition was kept constant at approximately 933 Pa by adjusting the pressure control valve. Methane ($CH_4$), hydrogen ($H_2$) and argon (Ar) gases were fed into the plasma head via set of mass flow controllers (MKS Instruments Ltd.). The gases were broken down remotely by the supplied MW power to form a plasma consisting of a high number of radicals that were delivered towards the substrate. The silicon wafer substrates (P(Boron) <100>, ~0.7 mm thick, Pi-Kem Ltd.) were placed underneath the plasma head on an adjustable height substrate holder made from anodised aluminium, providing good thermal conductivity and electrical inertness. The adjustable substrate holder allowed the distance between the substrate and the plasma to vary from 180 to 200 mm (see Fig. 1 for details). The operating temperature at the substrate holder was measured using a K-type thermocouple, which was attached to the substrate holder next to the Si wafer substrate, and VG was deposited directly onto Si wafer substrates. Prior to deposition the Si wafer was cleaned in an Ar plasma for 15 minutes, allowing the Si substrate to heat up to the operational temperature range. Table 1 summarises the conditions used during the cleaning and deposition processes.

Table 1: Process conditions adopted in this study.

| **Step** | **Synthesis time (min.)** | **MW Power (W)** | **Plasma to substrate distance (mm)** | **Gas flow rate (sccm)** | **Pressure (Pa)** |
|---|---|---|---|---|---|
| Ar Cleaning | 15 | 2800 | 180 – 200 | Ar = 1000 | 933 |
| VG Deposition | 5 – 40 | 2000 – 2500 | 180 – 200 | Ar = 1000<br>$H_2$ = 800<br>$CH_4$ = 80 – 200 | 933 |

### 2.3 Physicochemical characterisation

Raman spectroscopy (Renishaw inVia) was carried out using the 514.5 nm excitation wavelength of an argon ion laser at 10 % of its full power to avoid damaging the samples. Each spectrum is a record of three scans accumulated over 10 seconds exposure time at selected points of the sample surface.

Scanning electron microscopy (SEM, Zeiss Supra 40VP) was used in this study to determine the surface and cross-sectional morphology of the as-synthesised vertically oriented graphene. The SEM is equipped with a field emission cathode as an electron source and two different detectors (SE2 and InLens). The samples were analysed at an acceleration voltage of 3.0 kV and a working distance of 3.0 mm. In order to characterize the sample cross section, the coatings were fractured using liquid nitrogen.

A High-Resolution Transmission Electron Microscope (HRTEM, FEI Talos F200A) was used to obtain the microstructure of VG synthesised by MW-CVD as well as number of layers in the VG sheet. Graphene flakes were lifted out from the substrate, diluted in methanol, ultrasonificated and pipetted onto copper grids with a carbon film (Agar Scientific). TEM images were acquired under 200 kV acceleration voltage.

X-ray photoelectron spectroscopy (XPS) was performed to obtain the information about the chemical state of the elements in the samples. VG samples were analysed using an Axis Supra+ X-ray photoelectron spectrometer (Kratos Analytical Ltd.) equipped with Al Kα X-ray source. The binding energy values of XPS lines were calibrated using the C 1s peak of adventitious carbon at 284.8 eV as a reference. Data interpretation was carried out using CasaXPS software v2.3.18.

### *2.4 Electrochemical characterisation*

Cyclic voltammetry (CV) was used to determine the heterogeneous electron transfer coefficient ($k^o$) and the electroactive area ($A_{active}$) of the fabricated VG samples, measurements were carried out using an AUTOLAB PGSTAT101 driven by NOVA 2.0 software. Electrochemical testing was conducted in a typical three-electrode system, which consisted of a coiled Pt wire counter electrode, a saturated Ag/AgCl reference electrode and the synthesised VG as the working electrode. Note that the geometric area of the VG working electrodes was delimited to be 3.2 mm$^2$. The electrochemical area of the VG working electrodes was determined using a solution of 1 mM $[Ru(NH_3)_6]^{3+/2+}$ and 0.1 M KCl, which was degassed with nitrogen before the experiments. A potential window of -0.2 to -0.6 V was used for the CVs whilst 10 distinct scan rates from 5 to 500 mV s$^{-1}$ were sequentially implemented.

The electrochemically active area ($A_{active}$), was calculated from the Randle-Sevcik equation: $i_{p^{quasi}} = \pm 0.436 nFA_{active}C(nFD_{Ru}\nu/RT)^{\frac{1}{2}}$. In the equation the $i_p$ is the cathodic current peak, $n$ is the number of electrons involved in the reduction, $C$ is the concentration of the solution, $D_{Ru}$ is the diffusion coefficient for $Ru(NH_3)_6^{3+/2+}$ ($9.1\times10^{-6}$ cm$^2$ s$^{-1}$), $\nu$ is the scan rates, $F$ being the Faraday constant, $R$ being the gas constant and $T$ is the temperature in Kelvin [43-46]. The $A_{active}$ is widely used in graphene-based materials research [47, 48], and it is calculated from the slope of the $i_p$ versus $\nu^{1/2}$ curves.

In order to estimate the heterogeneous electron transfer (HET) constant $k^o$ of the VG working electrodes, the Nicholson method was employed [49], allowing to determine φ (kinetic parameter): $\varphi = k^0[\pi Dn\nu F/RT]^{-1/2}$. In Nicholson equation $D$ is the diffusion coefficient of the analyte (in this case $9.1\times10^{-6}$ cm$^2$ s$^{-1}$ for $[Ru(NH_3)_6]^{3+/2+}$). φ can be deduced from the peak to peak separation ($\Delta E_P$) of a single electron transfer faradaic process (at 298 K) given that : $\varphi = (-0.6288 + 0.0021\,X)/(1-0.017X)$, where $X = \Delta E_P$. A plot of $[\pi Dn\nu F/RT]^{-1/2}$ against φ yields a value for a standard heterogeneous rate constant, HET ($k^o$). If $\Delta E_P$ exceeds 212 mV the following formula should be implemented: $[2.18\,(\alpha Dn\nu F/RT)^{\frac{1}{2}}]\exp\,[-(\alpha^2 nF/RT)\times\Delta E_P]$, where $\alpha$ is assumed to be 0.5 [50, 51].

## 3. Results and discussion

### *3.1 VG growth and morphology*

The synthesis of VG through MW-CVD did not require any catalyst and the remote plasma allowed the deposition to take place at significantly lower temperatures when compared to other studies [18, 52, 53]. It is believed that the plasma environment affects the growth of graphene by influencing the energy (and therefore mobility) of active species like ions and electrons at different pressures, gas composition or applied power. Moreover, the microwave frequency promotes the formation of radicals within the plasma bulk, species, which are known for being extremely reactive. Vishwakarma et al. attempted to explain the possible growth mechanism of VG networks at low temperatures based on the hydrogen shifting reaction, which due to its great catalytic activity forms $C_nH_y$ species in the hot region of the plasma [32]. Authors also pointed out the importance of the Ar carrier gas in plasma ionisation by providing high energy electrons. Therefore, the VG was deposited directly on Si wafer with no additional substrate heating or biasing, eliminating the transfer step employed in the growth of graphene on catalytic substrates, such as Cu. To investigate the growth mechanism of the synthesised VG, the effect of several parameters on the film structure, such as deposition time, power, substrate distance from the plasma and gas ratio, were evaluated. Fig. 2 a-d) shows Raman spectra obtained from VG samples deposited under variable operating parameters.

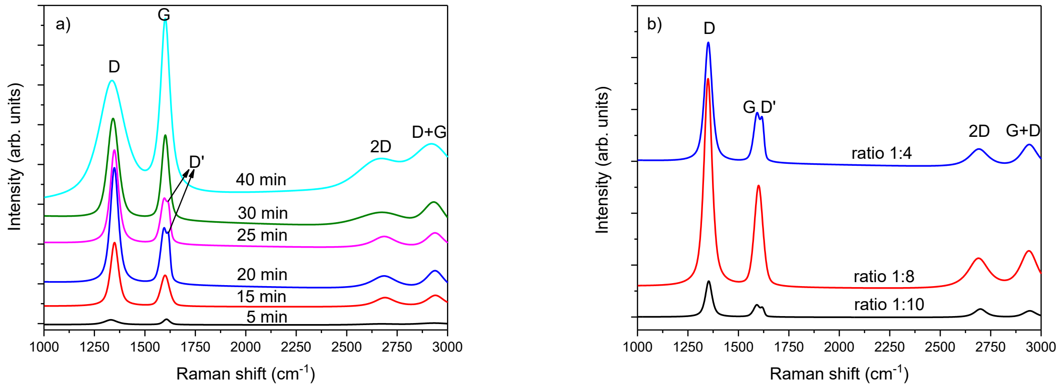

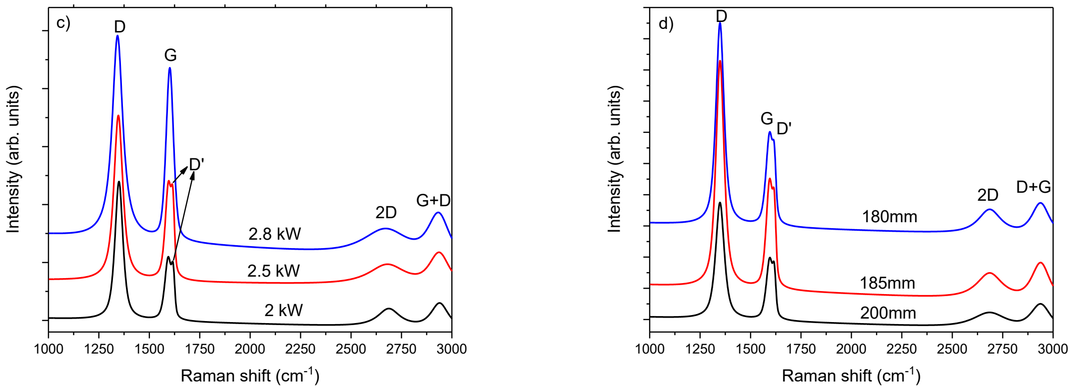

Figure 2: Raman results for the time-dependent growth of VSG a); the effect of MW power b), gas ratio c) and plasma to substrate distance d). Unless specified otherwise the remaining parameters were kept constant: gas ratio 1:8, pressure 933 Pa and plasma to substrate distance 185 mm, MW power 2.5 kW, deposition time 15 min.

In Fig. 2 a) Raman spectra were obtained from the samples deposited for different times, from 5 up to 40 minutes, while the other parameters were kept constant (1:8 $CH_4$:$H_2$, 933 Pa, 2.5 kW and 15 mm, respectively). It is clear that the shape and intensity of the peaks change with deposition time, and short-time synthesis (i.e. 5 min) is not sufficient to form VG. On the other hand, if the deposition time is too long the samples start to become amorphous, which is indicated by the broadening of the peaks. The effect of gas flowrate ratio on the growth mechanism of the VG is illustrated in Figure 2 b). The $CH_4$:$H_2$ ratios were adjusted to 1:4, 1:8 and 1:10, respectively. The intense peaks observed for the composition 1:8 indicate that this sample has a higher degree of crystallinity than samples deposited under the remaining gas ratios, 1:4 and 1:10, respectively. Fig. 2 c) shows Raman shifts from VG obtained for the three powers tested: 2, 2.5 and 2.8 kW. The power applied affected the synthesis temperature measured by the thermocouple at the substrate holder and resulted in intensity differences of the G-band, related to the D-band, indicating that the defect content varies with MW power. Moreover, at 2.8 kW power the D'-band is not visible, which could be explained by the merging of G and D' peaks at high defect concentration, due to the highest bombardment rates of the active species in the plasma, such as electrons or radicals, at higher power. Finally, adjusting the height of the substrate allowed VG deposition at shorter sample-to-plasma distances, which as a consequence increased substrate temperature from 275°C at 200 mm sample-to-plasma distance to 336°C at 180 mm sample-to-plasma distance, under otherwise identical conditions. As obtained from Raman analysis, reducing the sample-to-plasma distance from 200 mm to 185 mm and 180 mm, respectively, improves the crystallinity of the samples, as indicated by the sharp peaks observed in Fig. 2 d).

The Raman spectrum for graphene has three prominent bands: G-band at 1582 $cm^{-1}$, 2D-band at approximately 2700 $cm^{-1}$ and D-band at 1350 $cm^{-1}$ [54] and the Raman results from VG samples presented in Fig. 2 consists of five main peaks, namely: D (1350 $cm^{-1}$), G (1595 $cm^{-1}$), D' (1620 $cm^{-1}$) 2D (2680 $cm^{-1}$) and G+D (2940 $cm^{-1}$). This is related to the introduction of disorder (i.e. the graphene edges) that breaks the crystal symmetry of graphene and activates vibrational modes that otherwise would be silent, such as the D-band, D'-band and D+G-band [55]. The G-band indicates the graphitic characteristic of the material, i.e. its ability to conduct electricity and the broadened line width observed for 2D can be attributed to the relaxation of double resonance in Raman and is related to the random orientation of graphene sheets [56]. The D-band is attributed to the disorder-induced phonon mode and reflects the presence of disorder in $sp^2$ hybridised carbon materials [57]. The high intensity peak observed at approximately 1350 $cm^{-1}$ in most of the samples is due to the large fraction of carbon edges breaking the symmetry of the lattice. These types of defect are correlated to the enhanced adsorption and electron transfer process in graphene-related materials [12]. Thus, the presence of defects attributed to the D-band is important for the electrochemical activity of VG. As stated by Ferrari and Robertson [58], the Raman spectrum depends mainly on $sp^2$ content (i.e. presence of $sp^2$ rings or chains), bond disorder and $sp^2/sp^3$ ratio, also known as the amorphisation model. The transformation of graphite to amorphous carbon is described through three stages: (i) graphite to nanocrystalline graphite (NG); (ii) NG to low $sp^3$ amorphous carbon; (iii) low $sp^3$ amorphous carbon to high $sp^3$ amorphous carbon. The G peak is just related to the relative amount of $sp^2$ carbons and therefore, it is assumed to be constant as a function of disorder [59]. However, the D-band intensity is different in each stage and it characterizes two regimes: low defect regime (attributed to stage (i)) and high defect regime (attributed to stage (ii)). It is established that $I_D$ is directly proportional to the amount of defects in stage (i) and inversely proportional to defects in stage (ii).

Fig. 3 shows the evolution of the peak ratio $I_D/I_G$, which increases with deposition time up to 25 minutes of deposition, following by a significant decrease. The ratio between D and G ($I_D/I_G$) provides information about the amount of defects and disorder in the films, therefore this behaviour suggests that there are two disorder-induced mechanisms competing, and can be explained by the amorphisation model of graphitic materials [58]. Long synthesis times lead to the transformation of $sp^2$ content to $sp^3$ amorphous carbon, as found from Raman peak ratio analysis. Hence, the increase of $I_D/I_G$ ratio up to 25 minutes corresponds to stage (ii) and samples deposited for 15 minutes demonstrate the highest defect content observed in the time-dependent analysis. Longer deposition times (> 25 minutes) are described by stage (i), i.e. the low defects regime. Moreover, the broadening of the peaks shown by the FWHM values in Table 2 can be attributed to the relaxation of double resonance in Raman scattering due to the random orientation of the graphene layers [27]. Therefore, based on Raman peak analysis the optimum deposition time lies within 15 and 25 minutes with sample deposited for 15 minutes contains the highest content of defects (i.e. largest $I_D/I_G$ ratio).

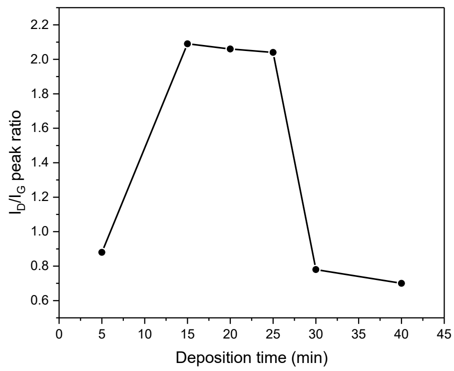

Figure 3: $I_D/I_G$ Raman shift intensity evolution as a function of deposition time. The remaining synthesis parameters were kept constant: gas ratio 1:8, pressure 933 Pa and plasma to substrate distance 185 mm, MW power 2.5 kW.

Table 2: Full width at half-maximum (FWHM) and peak ratio analysis of D, G and 2D-Band for the deposition time study. Except for deposition time, synthesis parameters were kept constant: gas ratio 1:8, pressure 933 Pa and plasma to substrate distance 185 mm, MW power 2.5 kW.

| Deposition time (min.) | Peak position | | | FWHM ($cm^{-1}$) | | | $I_D/I_G$ |
|---|---|---|---|---|---|---|---|
| | **D** | **G** | **2D** | **D** | **G** | **2D** | |
| 5 | 1333.33 | 1607.04 | 2667.72 | 78.12 | 39.01 | 237.02 | 0.88 |
| 15 | 1349.58 | 1598.96 | 2689.35 | 47.98 | 48.45 | 124.16 | 2.09 |
| 20 | 1350.41 | 1595.41 | 2689.93 | 46.78 | 43.43 | 123.95 | 2.06 |
| 25 | 1349.49 | 1594.91 | 1685.93 | 48.25 | 40.17 | 155.39 | 2.04 |
| 30 | 1335.00 | 1603.70 | 2659.82 | 92.80 | 43.14 | 271.85 | 0.78 |
| 40 | 1335.34 | 1601.32 | 2659.44 | 140.15 | 55.63 | 244.19 | 0.70 |

The gas ratio study showed that for the 1:10 gas composition the low intensity of the G-band indicates poor graphitic structure. For the $CH_4$ rich gas composition (ratio 1:4), on the other hand, black powders were observed on the substrate and the spectra recorded in the Raman indicated the presence of amorphous carbon and in some areas of nucleation islands of VG, as shown in the SEM image in Fig. 4 a). By adjusting the gas ratio to an intermediate composition (i.e. 1:8 ratio), a significant improvement in the crystallinity of the samples was observed, as indicated by the intense peaks in the Raman spectra presented in Fig. 2 b) and a typical flower-like VG structure in Fig. 4 b). Excess of $CH_4$ in the gas mixture facilitates amorphous carbon formation with only several nucleation sites for VG, as shown in the form of graphene islands in Fig. 4 a). It is believed that the growth of VG is a competing process between etching amorphous carbon by $H_2$ and forming nucleating graphene islands. The synthesis involves three critical steps, which are in brief: the adsorption of hydrocarbon building units and nucleation of a graphene buffer layer on the substrate surface, the vertical growth directed by the electric field within the plasma discharge, and a termination step due to graphene edges naturally ceasing at a closed edge [5, 60, 61]. Thus, the composition 1:8 resulted in a balance between these two events, leading to the growth of crystalline $sp^2$ carbon with vertical orientation.

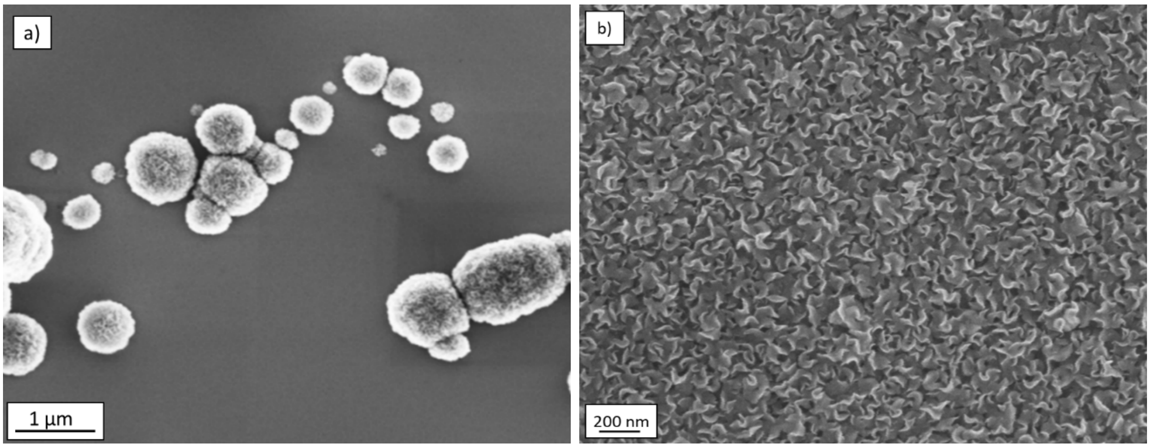

Figure 4: SEM images for of the top view of VG deposited in $CH_4$ – rich atmosphere, ratio 1:4 a) and at gas ratio 1:8 b), deposited for 15 min at pressure 933 Pa and plasma to substrate distance 185 mm, MW power 2.5 kW.

Moreover, Raman spectra for VG synthesized using the composition 1:8 did not show the D' peak. D and D' bands are only active in the near vicinity of defects. Especially for the D' peak, there are only a few studies discussing its origin [57, 62]. In general this peak has a relatively low intensity when compared to the D-band, and at sufficient high defect concentrations the

D’ peak starts to merge with the G-band [57]. Thus, it becomes difficult to separate the contribution of G and D’-bands, as observed for the ratio 1:8. However, the work carried out by Eckmann et. al [57] showed that the $I_D/I_{D'}$ ratio can also give information about defect type, such as hopping defects, on-site defects and charged impurities. These three types of defects are produced by the deformation of the carbon bonding, out-of-plane atoms bonded to carbon atoms (i.e. C with $sp^3$ hybridization) or charged species adsorbed on the graphene sheet, respectively.

Fig. 5 a-d) presents the evolution of VG morphology with deposition time observed in the SEM. It was found that when the deposition time was increased the exposed network of VG was gradually compromised, until the organization was no longer observed after 30 minutes of synthesis. The cross-section images shown in the insets also show the exposed edges and the vertical orientation of the coating, however, no organisation was observed in the sample synthesised for 30 minutes (Fig. 5 d)). This is due to the longer exposure of vertically growing walls to high-energy ion bombardment sintering amorphisation. Moreover, the sample deposited for 15 minutes exhibits the thinnest nanosheets and the highest content of defects, which is indicated by the highest $I_D/I_G$ ratio in the Raman analysis (see Table 2 and Fig. 3 for details).

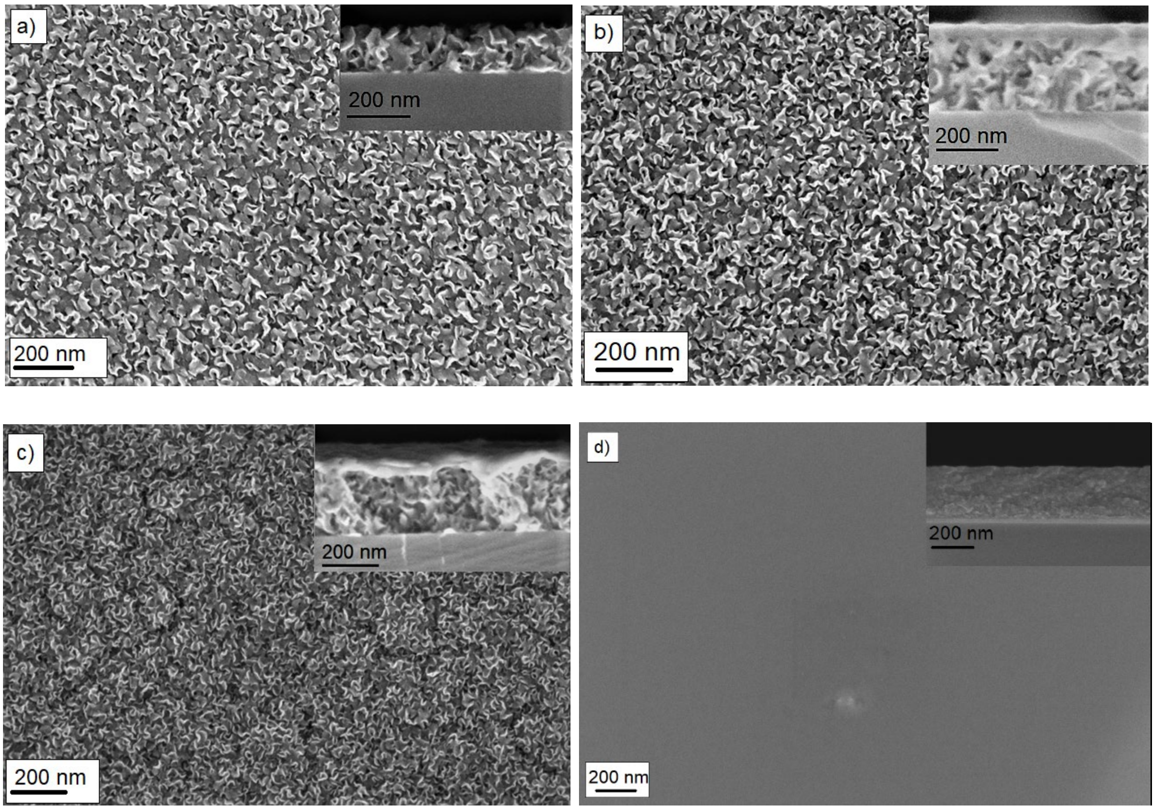

Figure 5: SEM images for the time-dependent analysis, showing the top view of the samples and the cross section (inset) deposited for 15 a), 20 b), 25 c) and 30 minutes d) at gas ratio 1:8, pressure 933 Pa and plasma to substrate distance 185 mm, MW power 2.5 kW.

Fig. 6 a-c) shows graphene deposited at variable powers, but under constant remaining synthesis parameters. Increasing the MW power from 2 kW to 2.5 kW caused a significant rise in the thickness of the growing graphene film. At 2 kW power the thickness measured was approximately 40 nm, whereas at 2.5 kW it was approx. 200 nm, which is a five-fold increase. There was no additional heater coupled to the substrate holder, therefore the temperature recorded by the thermocouple on the substrate holder shows the direct response to the applied power. The substrate temperature increases with power, which favours the growth kinetics of nanostructures and therefore the growth rate of VG increases with temperature, as shown in Fig. 6 a-b). At 2.8 kW, on the other hand, the sample showed no organisation, as can be seen in the cross sectional inset in Fig. 6 c). Since the applied MW power is responsible for the degree of ionisation in the plasma and the heating of the substrate, it is believed that at higher powers the ionisation rate will increase causing faster film growth that will naturally cease at closed edges over time, densify the film and start damaging the nanostructures formed. The top surface in Fig. 6 c) also shows significantly thicker/denser nanosheets that appear to have a ‘noodle-like’ structures rather than thin flakes when comparing to remaining micrographs. The cross-section image in the inset also shows rather dense structure without the sign of vertically standing structures. The thick edges could be associated with the high intensity G-band obtained from Raman analysis shown in Fig. 2 c).

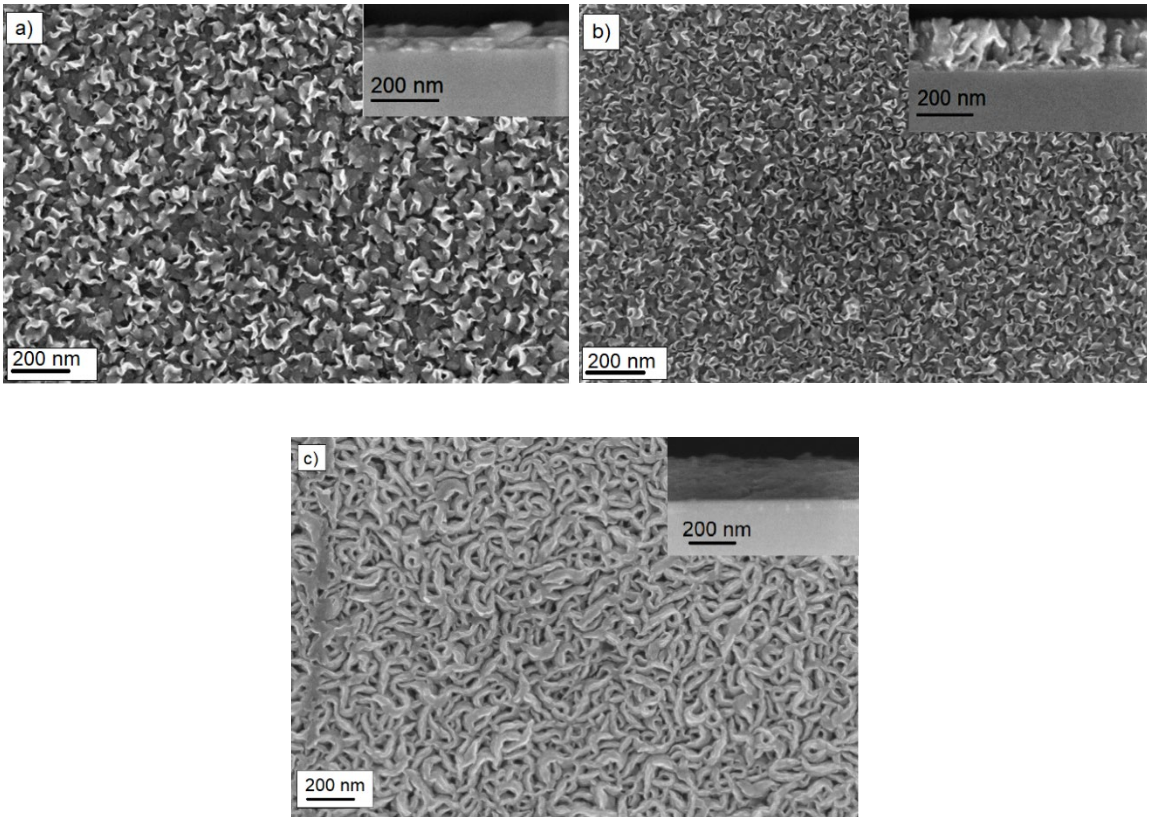

Figure 6: SEM images obtained from samples deposited under 2 kW a), 2.5 kW b) and 2.8 kW c) applied power, respectively. The remaining synthesis parameters were: gas ratio 1:8, pressure 933 Pa and plasma to substrate distance 185 mm, time 15 min.

Fig. 7 shows the SEM results collected from the samples deposited at 185 and 180 mm distance between the plasma and the substrate, respectively. It is noticeable that the distance from the plasma greatly affected the thickness of the VG samples and their morphology. When the distance between the substrate and plasma head was reduced from 185 to 180 mm the sample thickness increased from 180 nm to 596 nm, respectively, as shown in the insets in Fig. 7 a-b). This fact can be related to the higher deposition rates achieved at higher temperatures due to closer proximity to the plasma. However, decreasing the distance from plasma also resulted in a cauliflower like structure, as can be seen in the top view images in Fig. 7 b). According to Ostrikov et al. [61], the morphology of nanostructures formed in PECVD systems depends on supply and consumption of precursors, whereby the consumption depends on the substrate temperature. Since all the other parameters were kept constant, the substrate temperature is determined by the distance from the plasma. Thus, the morphology and thickness of VG synthesized through MW-CVD is influenced by the distance from the substrate to the plasma.

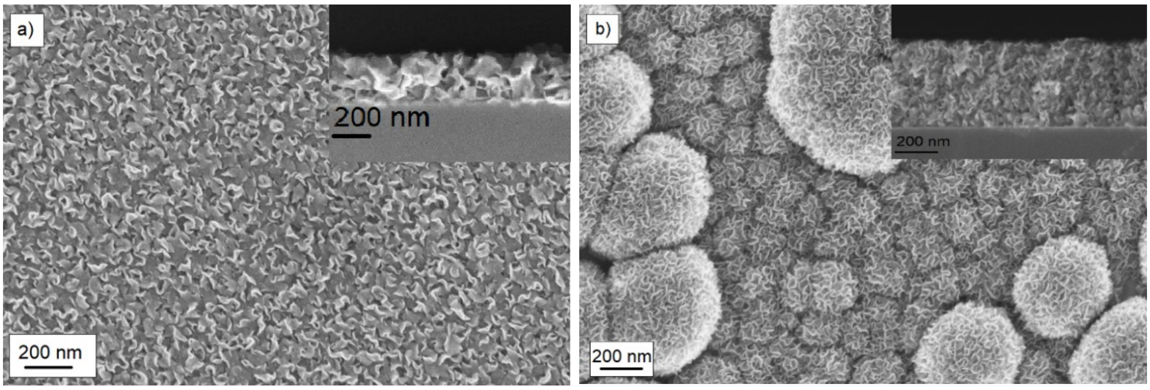

Figure 7: SEM images obtained from VG deposited at variable plasma to substrate distance of 185 nm a) and 180 mm b), respectively, at gas ratio 1:8, pressure 933 Pa, 2.5 kW applied power and synthesis time of 15 min.

Fig. 8 a) shows full view TEM image of the graphene flakes deposited for 25 minutes. HRTEM analysis depicted in Fig. 8 b-c) revealed that the graphene flakes consist of several (~5-20) layers of graphene. Moreover, Fig. 8 c) shows a typical tapered edge of VG described in details elsewhere [5]. It is believed that tapered edges are commonly observed in VG structures and such arrangements between the layers could cease the growth mechanism of VG. This in turn, could lead to VG growth termination according to the amorphisation model of graphitic materials, if the synthesis time increased beyond 25 minutes, which supports hypothesis described in Fig. 3.

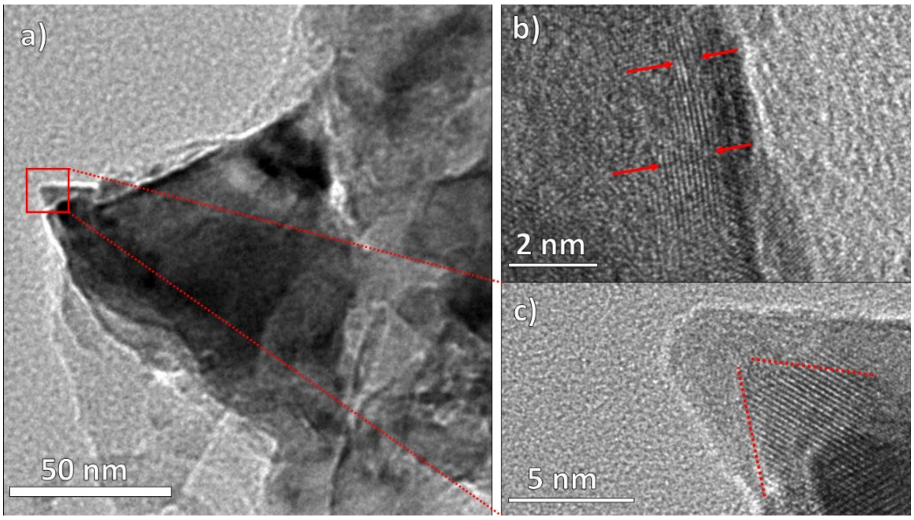

Figure 8: a) Full view TEM image of VG graphene flakes deposited by MW-CVD; b) HRTEM image showing the edge of the VG consisting of a few layers of graphene; c) The inset of the magnified edge in a) is a HRTEM image showing relatively thick (~20 layers) tapered edge of VG. Sample was synthesised at gas ratio 1:8, pressure 933 Pa, power 2.5 kW, plasma to substrate distance 185 mm and synthesis time of 25 min.

### *3.2 Electrochemical Characterisation*

As described in the experimental section cyclic voltammetry (CV) was implemented to explore the electrochemically active area of a VG working electrodes using the near ideal outer sphere redox probe 1 mM $[Ru(NH)_6]^{3+}$ / 0.1M KCl. [63]. The obtained CVs were used to determine the electrochemical area and the heterogeneous electron transfer coefficient ($k^o$). The results collected from samples deposited for 15 and 20 minutes at plasma to substrate distance of 185 and 180 mm were obtained from a range of voltammetric scan rates study, as presented in Fig. 9 a-d). Samples were synthesised at MW power of 2.5 kW, gas ratio 1:8 ($CH_4$:$H_2$) and a pressure of 933 Pa. The insets present the analysis of the current peak as a function of scan rate.

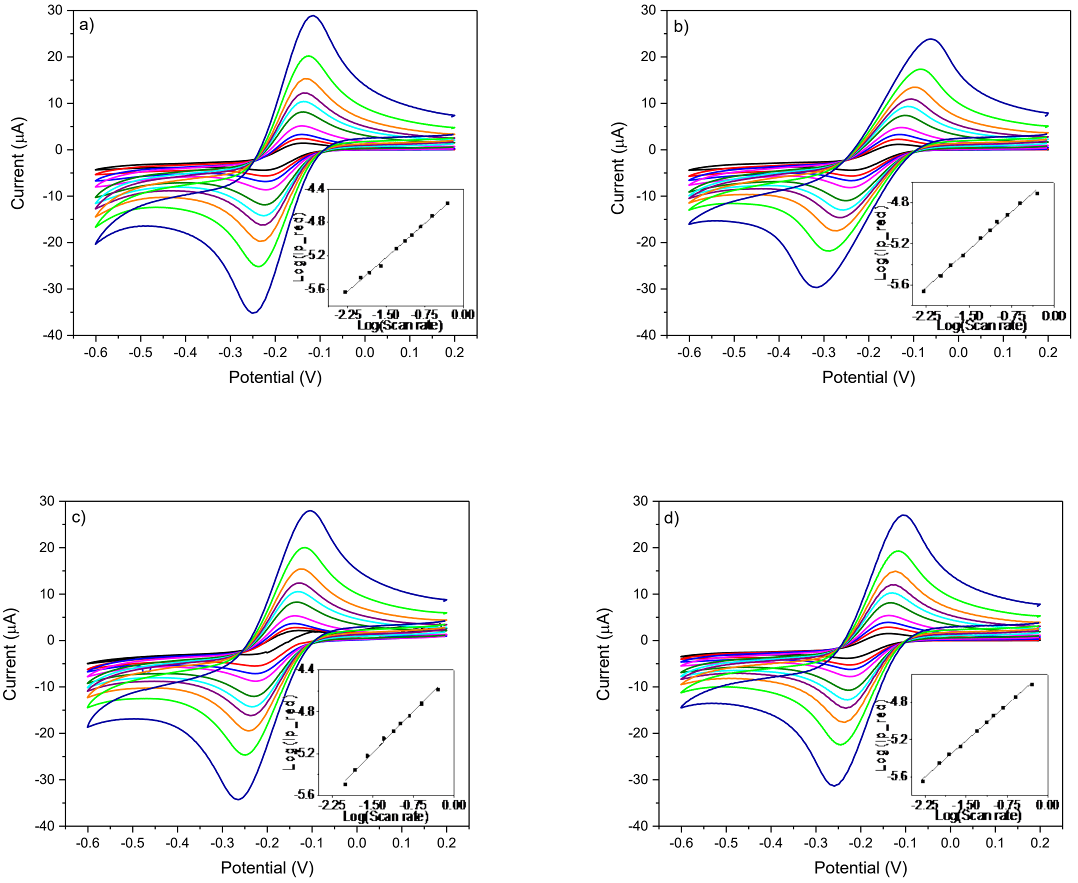

Figure 9: CV profiles recorded using 1 mM $[Ru(NH_3)_6]^{3+/2+}$ in 0.1 M KCl, at different scan rates for VG grown at h = 15 mm for 15 minutes a) and 20 minutes b) and at h = 20 mm for 15 minutes c) and 20 minutes d), respectively. The insets present the analysis of the current peak as a function of scan rate. Remaining synthesis parameters were: gas ratio 1:8, pressure 933 Pa, power 2.5 kW.

It was previously observed that porous structures may give an apparent improvement in the voltammetric response, which gives rise to misinterpretation of the electro-catalytic nature of the sample [64]. This event is known as the “thin layer effect” and it happens when electroactive species are trapped into electrodes with a porous structure, forming a ‘thin layer’ of solution that apparently increases the electrochemical response of the sample. To ensure that the voltammetric response obtained in this study is diffusional in nature, and not due to the thin layer effect, the peak current was monitored as a function of a scan rate. As seen in the inset graphs in Fig. 9 a-d), the linear response observed for these samples indicates that the electrochemical response is purely diffusional.

The electroactive areas ($A_{active}$) and $k^o$ values were calculated from the Randle-Sevcik equation for quasi-reversible process and Nicholson's method, respectively, as described in Experimental section, and are shown in Table 3. The geometric area ($A_{geo.}$) of the working electrode was fixed for all tests and corresponded to physical dimensions of 7.89x10$^{-2}$ cm$^2$. By dividing $A_{active}$ obtained from Randle-Sevcik equation by the $A_{geo.}$, it is possible to estimate how much of the surface area of VG is electrochemically active (%Real = $A_{active}/A_{geo.}$*100%) [45]. However, a deeper investigation of the specific surface area of VG is required to correlate the improved electrochemical properties with the porosity of synthesised films.

Table 3: Summary of the electrochemical properties of the VG synthesised in this study. Remaining synthesis parameters were: gas ratio 1:8, pressure 933 Pa and power 2.5 kW.

| **Sample number** | **Plasma to substrate distance (mm)** | **Deposition time (min)** | **$\Delta E_p$/mV (@100 mV s$^{-1}$)** | **HET ($k^o$;cm$^{-1}$)** | **$A_{active}$ (cm$^2$)** | **%Real** |
|---|---|---|---|---|---|---|
| VG-A | 185 | 15 | 119.6 | 3.68E-03 | 3.22E-02 | 41% |
| VG-B | 185 | 20 | 107.4 | 6.53E-03 | 3.49E-02 | 44% |
| VG-C | 180 | 15 | 100.1 | 6.09E-03 | 4.68E-02 | 59% |
| VG-D | 180 | 20 | 100.1 | 7.28E-03 | 4.51E-02 | 57% |

As the sample to plasma distance reduces from 185 to 180 mm there was a corresponding decrease in the obtained $\Delta E_p$, suggesting that, as the VG gets larger in vertical height its ability to effectively transfer electrons increases.

The lowest HET values obtained for the VG synthesized for 15 min at 185 mm away from the plasma bulk can be explained by it having a smaller ratio of active edge sites to inactive basal sites when compared to the remaining samples. VG grown for 15 and 20 min at a closer distance to the plasma present faster electron transfer kinetics when compared to the samples synthesised at 185 mm distance from the plasma for the same time. The deposition times of 15 and 20 minutes, on the other hand, were found to have a smaller influence on the electron transfer abilities of the samples. As shown in Table 3, the electroactive area in samples deposited for 15 minutes consists of just above 40% of the total sample area subjected to the cyclic voltammetry test, whereas samples synthesized for 20 minutes show electroactive areas of nearly 60%. The average 20% difference in electroactive area in samples deposited at these plasma-to-substrate distances could be attributed to the deposition temperature, which was recorded to be approximately 60°C higher for the samples synthesised closer to the plasma. The growth temperature of VG is a critical parameter and directly affects the surface reaction kinetics [25, 65]. The temperature uniformity influences not only the nucleation rate, but also the film crystallinity, composition, mechanical properties and electrical transport properties [27, 66, 67]. For this reason, several authors have used external heaters coupled with the substrate holder aiming to keep the growth temperature constant [68, 69]. Thus, faster deposition rates are achieved at higher temperatures, which significantly increased the VG thickness to 596 nm and the surface area displayed cauliflower-like structures in Fig. 7, which could benefit the electrochemical transfer of the VG structures. However, Brownson et al. has shown that increased mass of graphene results in increased $\Delta E_p$ [70], which could imply that the unhindered graphene networks and exposed electrochemically active edges could lead to an improvement in the HET and $A_{active}$ in this study.

The synthesized samples selected for electrochemical characterisation were analysed by XPS to further investigate the chemical states of the elements with respect to their functional groups. Fig. 10 a-d) shows de-convoluted high resolution XP spectra for C 1s collected from samples listed in Table 3, respectively. C 1s peaks show a typical graphite/graphene sp$^2$ structure with a tail visible at the higher energy end in every sample. The de-convoluted C 1s peaks consist of C=C at a binding energy of 284.5 eV, C-O at 286.0 eV and π-π* satellite bonds at 290.9 eV. The atomic concentrations of each corresponding carbon phase are assigned in the spectra.

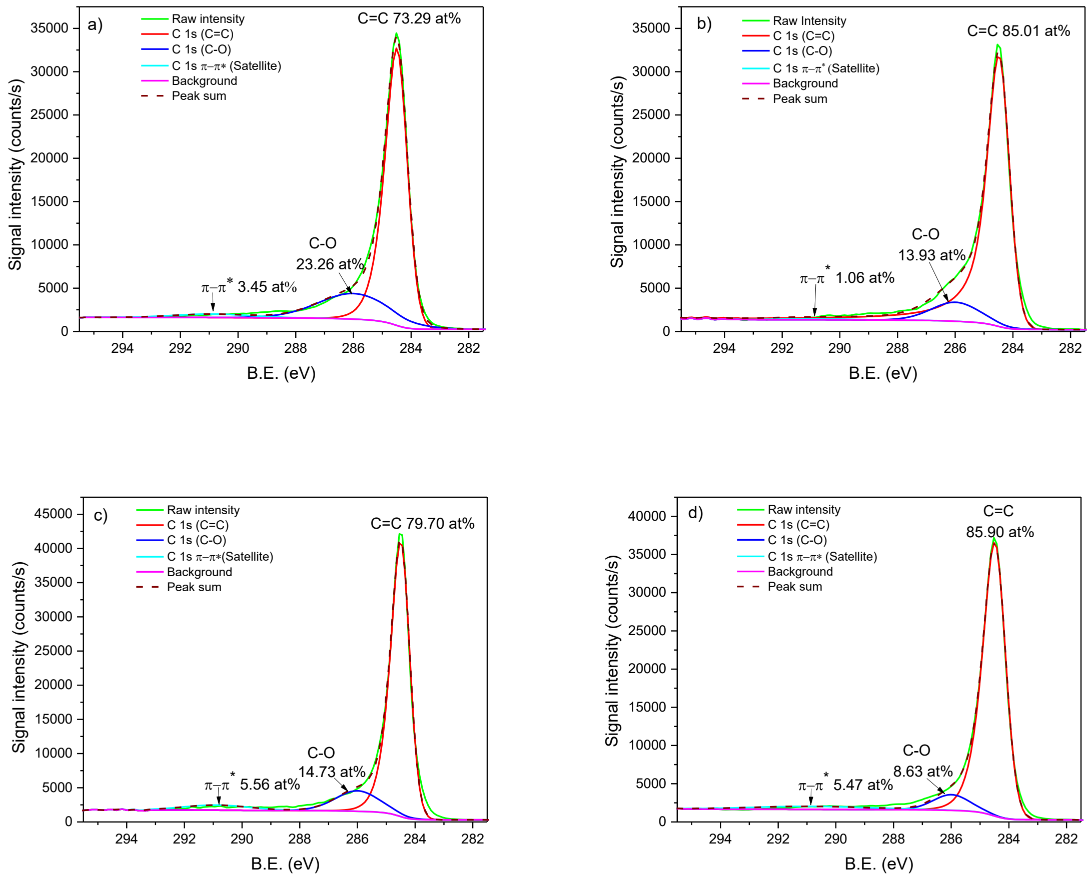

Figure 10: High resolution XPS spectra collected from sample VG-A a), VG-B b), VG-C c) and VG-D d), respectively. C1s peaks have been de-convoluted and atomic concentration of each phase have been ascribed in graphs.

The XPS results revealed that the VG mainly consists of graphene C=C bonds, relatively small amount of graphene oxide on the surface indicated by C-O bonds and a π-π* shake-up satellite peak characteristic feature of $sp^2$ hybridization of carbon. The conductivity of $sp^2$ carbon is related to the availability of π-conjugate delocalized electrons, therefore it could be considered that as the amount of π-π* increases, so does the electrical conductivity [71, 72]. This agrees with findings obtained in this study, as the lowest concentrations of the satellite peaks were detected in samples VG-A and VG-B synthesised for 15 minutes, which also showed the slowest electron transfer (increased $\Delta E_p$ calculated from electrochemical tests shown in Table 3).

## 4. Conclusions

In this study, it was demonstrated that the high-density plasma created by a microwave power supply provides enough energy to heat the substrates, allowing direct deposition of VG on non-catalytic substrates, such as Si wafers. The synthesis of the VG at temperatures in the range of 300°C opens up the possibility for direct synthesis of graphitic materials onto temperature-sensitive substrates, such as polymers. Based on Raman and SEM analysis it was demonstrated that deposition parameters, such as deposition time, gas ratio, power and substrate distance from the plasma influence the growth of vertical graphene structures. The deposition temperature, which is a result of the applied MW power, resulted in increased defect content at higher MW power and thicker VG. This could be attributed to enhanced film growth at higher synthesis temperature, which favours the growth kinetics of VG nanostructures. Whereas the prolonged synthesis time in close proximity to the highly energetic plasma (smaller substrate-to-plasma distance, increased synthesis temperature) could lead to amorphisation of the structure and undesired $sp^2$ to $sp^3$ transitions. Finally, the $CH_4$:$H_2$ gas ratio plays an important role in VG formation, as the synthesis is a competition between the etching process of amorphous carbon by $H_2$ and the growth of graphene. Therefore, the operating conditions must be tailored to achieve a balance between these two events in order to grow crystalline $sp^2$ carbon with vertical orientation.

The CV analysis showed that samples synthesized for 15 and 20 minutes at 185 and 180 mm distance from the plasma are rather similar and characteristic of quasi-reversible processes. VG grown for 15 and 20 min at smaller distances to the plasma showed faster electron transfer kinetics and higher electroactive areas when compared to the samples synthesised at a larger distance for the same time. The VG synthesised for 15 and 20 min at a distance of 185 mm away from the plasma showed fewer active sites when compared to the samples grown for the same time, but closer to the plasma, which is indicated by the reduction in the percentage of available active sites.

Finally, XPS analysis revealed that the VG mainly consists of graphitic $sp^2$ hybridized C=C bonds showing characteristic tail at higher energy levels. The atomic concentration of the satellite peaks at 290.9 eV could affect the electrochemical performance of the samples, as obtained from cyclic voltammetry test.

## Acknowledgements

Manchester Fuel Cell Innovation Centre was partially funded by European Regional Development Fund (ERDF) under the grant number 15R16P01182.

Special thanks to James Kelly, who during his student work experience built a stand for the microwave plasma reactor and connected the water-cooling to the system.

## References:

1. Bo, Z., Yang, Y., Chen, J.,, Yu, K., Yana, J., Cen, K., *Plasma-enhanced chemical vapor deposition synthesis of vertically oriented graphene nanosheets.* Nanoscale, 2013. **5**: p. 5180-5204.
2. Chen, J., Bo, Z., Lu, G., *Vertically-Oriented Graphene PECVD Synthesis and Applications*. 2015, Switzerland: Springer International Publishing.
3. Davami, K., Shaygan, M., Kheirabi, S., Zhao, J., Kovalenko, D. A., Rummeli, M. H., Opitz, J., Cuniberti, G., Lee, J.-S., Meyyappan, M., *Synthesis and characterization of carbon nanowalls on different substrates by radio frequency plasma enhanced chemical vapor deposition.* Carbon, 2014. **72**: p. 372-380.
4. Ghosh, S., Polaki, S. R., Kumar, S., Amirthapandian, S., Kamruddin, M., Ostrikov, K., *Process-specific mechanisms of vertically oriented graphene growth in plasmas.* Beilstein J. Nanotechnol., 2017. **8**: p. 1658–1670.
5. Zhao, J., Shaygan, M., Eckert, J., Meyyappan, M., Rümmel, M. H., *A Growth Mechanism for Free-Standing Vertical Graphene.* Nano Letters, 2014. **14**: p. 3064−3071.
6. Novoselov, K.S., A. K. Geim, A. K., Morozov, S. V., Jiang, D., Zhang, Y., Dubonos, S. V., Grigorieva, I. V., Firsov, A. A., *Electric Field Effect in Atomically Thin Carbon Films.* Science, 2004. **306**: p. 666-669.
7. Balandin, A.A., *Thermal properties of graphene and nanostructured carbon materials.* Nature Mat., 2011. **10**: p. 569-581.
8. Lee, C., Xiaoding Wei, X., Kysar, J. W., Hone, J., *Measurement of the Elastic Properties and Intrinsic Strength of Monolayer Graphene.* Science, 2008. **321**: p. 385-388.
9. Lehmann, K., Yurchenko, Ol., Heilemann, A., Vierrath, S., Zielke, L., Thiele, S., Fischer, A., Urban, G.,, *High surface hierarchical carbon nanowalls synthesized by plasmadeposition using an aromatic precursor.* Carbon, 2017. **118**: p. 578-587.
10. Zhou, H., Liu, D., Luo, F., Luo, B., Tian, Y., Chen, D., Shen, C., *Preparation of graphene nanowalls on nickel foam as supercapacitor electrodes.* Micro & Nano Letters, 2018. **13**(6): p. 842-844.
11. Han, C.-P., Veeramani, V., Hsu, C.-C., Jena, A., Chang, H., Yeh, N.-C., Hu, S.-F., Liu, R.-S., *Vertically-aligned graphene nanowalls grown via plasma-enhanced chemical vapor deposition as a binder-free cathode in Li–O2 batteries.* Nanotechnology, 2018. **29**.
12. Brownson, D.A.C., Banks, C. E., *The electrochemistry of CVD graphene: progress and prospects.* Phys. Chem. Chem. Phys., 2012. **14**: p. 8264–8281.
13. Banks, C.E., Compton, G. C., *New electrodes for old: from carbon nanotubes to edge plane pyrolytic graphite.* The Analyst, 2006. **131**: p. 15-21.
14. Bo, Z., Mao, S., Han, Z. J., Cen, K., Chen, J., Ostrikov, K., *Emerging energy and environmental applications of vertically-oriented graphenes.* Chem. Soc. Rev., 2015. **44**: p. 2108-2121.
15. Bo, Z., Hu, D., Kong, J., Yan, J. Cen, K., *Performance of vertically oriented graphene supportedplatinumeruthenium bimetallic catalyst for methanol oxidation.* J. Power Sources, 2015. **273**: p. 530-537.
16. Kamat, P.V., *Graphene-Based Nanoarchitectures. Anchoring Semiconductor and Metal Nanoparticles on a Two-Dimensional Carbon Support.* J. Phys. Chem. Lett., 2010. **1**: p. 520-627.

17. Kumar, S., van der Laan, T., Rider, A. E., Randeniya, L., Ostrikov, K., *Multifunctional Three-Dimensional T-Junction Graphene Micro-Wells: Energy-Efficient, Plasma-Enabled Growth and Instant Water-Based Transfer for Flexible Device Applications.* Adv. Funct. Mater., 2014. **24**: p. 6114–6122.
18. Boyd, D.A., Lin, W.-H., Hsu, C.-C., Teague, M. L., Chen, C.-C., Lo, Y.-Y., Chan, W.-Y., Su, W.-B., Cheng, T.-C., Chang, C.-S., Wu, C.-I., Yeh, N.-C., *Single-step deposition of high-mobility graphene at reduced temperatures.* Nature Communication, 2015. **6**: p. 1-8.
19. Li, X., Cai, W., An, J., Kim, S., Nah, J., Yang, D., Piner, R., Velamakanni, A., Jung, I., Tutuc, E., Banerjee, S. K., Colombo, L., Ruoff, R. S., *Large-Area Synthesis of High-Quality and Uniform Graphene Films on Copper Foils.* Science, 2009. **324**: p. 1312-1314.
20. Li, X., Magnuson, C. W., Venugopal, A., An, J., Suk, J. W., Han, B., Borysiak, M., Cai, W., Velamakanni, A., Zhu, Y., Fu, L., Vogel, E. M., Voelkl, E., Colombo, L., Ruoff, R. S., *Graphene Films with Large Domain Size by a Two-Step Chemical Vapor Deposition Process.* Nano Letters, 2010. **10**: p. 4328–4334.
21. Yan, Z., Lin, J., Peng, Z., Sun, Z., Zhu, Y., Li, L., Xiang, C., Loic Samuel, E., Kittrell, C., Tour, J. M., *Toward the Synthesis of Wafer-Scale Single-Crystal Graphene on Copper Foils.* ACS Nano, 2012. **6**(10): p. 9110–9117.
22. Funer, M., Wild, C., Koidl, P., *Simulation and development of optimized microwave plasmareactors for diamond deposition.* Surf Coat Technol., 1999. **116-119**: p. 853-862.
23. Mankelevich, Y.A., May, P. W., *New insights into the mechanism of CVD diamond growth: Single crystal diamond inMW PECVD reactors.* Diamond & Related Materials, 2008. **17**: p. 1021-1028.
24. Shul, R.J., Pearton, S. J., *Handbook of Advanced Plasma Processing Techniques*. 2000, Berlin, Germany: Springe-Verlag.
25. Sun, J., Chen, Y., Cai, X., Ma, B., Chen, Z., Priydarshi, M. Kr., Chen, K., Gao, T., Song, X., Ji, Q., Guo, X., Zou, D., Zhang, Y., Liu, Z., *Direct low-temperature synthesis of graphene on various glasses by plasma-enhanced chemical vapor deposition for versatile, cost-effective electrodes.* Nano Research, 2015. **8**(11): p. 3496–3504.
26. Zhang, L., Shi, Z., Wang, Y., Yang, R., Shi, D., Zhang, G., *Catalyst-Free Growth of Nanographene Films on Various Substrates.* Nano Research, 2011. **4**(3): p. 315-321.
27. Jiang, L., Yang, T., Liu, F., Dong, J., Yao, Z., Shen, C., Deng, S., Xu, N., Liu, Y., Gao, H.-J., *Controlled Synthesis of Large-Scale, Uniform, Vertically Standing Graphene for High-Performance Field Emitters.* Adv. Mater., 2013. **25**: p. 250-255.
28. Li, M., Liu, D., Wei, D., Song, X., Wei, D., Wee, A. T. S., *Controllable Synthesis of Graphene by Plasma-Enhanced Chemical Vapor Deposition and Its Related Applications.* Adv. Sci., 2016. **3**.
29. Liu, J., Cao, G., Yang, Z., Wang, D., Dubois, D., Zhou, X., Graff, G. L., Pederson, L. R., Zhang, J.-G., *Oriented Nanostructures for Energy Conversion and Storage.* Chem. Sus. Chem., 2008. **1**: p. 676 – 697.
30. Wu, W.-M., Zhang, C.-S., Yang, S.-B., *Controllable synthesis of sandwich-like graphene -supported structures for energy storage and conversion.* New Carbon Materials, 2017. **32**(1): p. 1-14.
31. Angus, J.C., Wang, Y., Sunkara, M., *Metastable growth of diamond and diamond-like phases.* Annu. Rev. Mater. Sci., 1991. **21**: p. 221-248.

32. Vishwakarma, R., Zhu, R., Abuelwafa, A. A., Mabuchi, Y., Adhikari, S., Ichimura, S., Soga, T., Umeno, M., *Direct Synthesis of Large-Area Graphene on Insulating Substrates at Low Temperature using Microwave Plasma CVD.* ACS Omega, 2019. **4**: p. 11263-11270.
33. Shiji, K., Hiramatsu, M., Enomoto, A., Nakamura, M., Amano, H., Hori, M., *Vertical growth of carbon nanowalls using rf plasma-enhancedchemical vapor deposition.* Diamond & Related Materials, 2005. **14**: p. 831-834.
34. Hajati-Talemi, P., Simon, G. P., *Preparation of graphene nanowalls by a simplemicrowave-based method.* Carbon, 2010. **48**: p. 3993-4000.
35. Kim, Y., Song, W., Lee, S. Y., Jeon, C., Jung, W., Kim, M., Park, C.-Y. , *Low-tempearture synthesis of graphene on nickel foli by microwave plasma chemical vapour deposition.* Appl. Phys. Lett., 2011. **98**: p. 263106
36. Malesevic, A., Vitchev, R., Schouteden, K., Volodin, A., Zhang, L., Van Tendeloo, G., Vanhulsel, A., Van Haesendonck, C. , *Synthesis of few-layer graphene via microwave plasma-enhanced chemical vapour deposition.* Nanotechnology, 2008. **19**.
37. Suzuki, S., Chatterjee, A., Cheng, C.-L., Yoshimura, M., *Effect of Hydrogen on Carbon Nanowall Growth by Microwave Plasma-Enhanced Chemical Vapor Deposition.* Japanese Journal of Applied Physics, 2011. **50**.
38. Kalita, G., Wakita, K., Umeno, M., *Low temperature growth of graphene film by microwave assisted surface wave plasma CVD for transparent electrode application.* RSC Advances,, 2012. **2**: p. 2815–2820.
39. Kim, J., Ishihara, M., Koga, Y., Tsugawa, K., Hasagawa, M., Iijima, S., *Low-temperature synthesis of large-area graphene-based transparent conductive films using surface wave plasma chemical vapor deposition.* Appl. Phys. Lett., 2011. **98**: p. 091502.
40. Laan van der, T., Kumar, S., Ostrikov, K., *Water-mediated and instantaneous transfer of graphene grown at 220 °C enabled by a plasma.* Nanoscale, 2015. **7**: p. 20564-20570.
41. Peng, K.-J., Wu, C.-L., Lin, Y.-H., Liu, Y.-J., Tsai, D.-P., Pai, Y-.H., Lin, G.-R., *Hydrogen-free PECVD growth of few-layer graphene on an ultra-thin nickel film at the threshold dissolution temperature.* J. Mater. Chem. C, 2013. **1**: p. 3862-3870.
42. Zhang, Z., Lee, C.-S., Zhang, W., *Vertically Aligned Graphene Nanosheet Arrays: Synthesis, Properties and Applications in Electrochemical Energy Conversion and Storage.* Adv. Energy Mater., 2017. **7**: p. 1700678.
43. Bard, A.J., Faulkner, L. R., *Electrochemical Methods: Fundamentals and Applications* 2nd Edition ed. 1980, UK: Wiley.
44. Compton, R.C., Banks, C. E., *Understanding Voltammetry*. Third edition ed. 2018, London, UK: World Scientific Publishing Europe Ltd.
45. García-Miranda Ferrari, A., Foster, C. W., Kelly, P. J., Brownson, D. A. C., Banks, C. E., *Determination of the Electrochemical Area of Screen-Printed Electrochemical Sensing Platforms.* Biosensors, 2018. **8**(2): p. 53.
46. Matsuda, H., Ayabe, Y., *Zur Theorie der Randles-Sevčikschen Kathodenstrahl-Polarographie.* Berichte der Bunsengesellschaft fur physikalische Chemie, 1955. **59**(6): p. 494-503; reference in German.
47. Foster, C.W., Down, M. P., Zhang, Y., Ji, X., Rowley-Neale, S. J., Smith, G. C., Kelly, P. J., Banks, C. E., *3D Printed Graphene Based Energy Storage Devices.* Scientific Reports, 2017. **7**.

48. Lehmann, K., Yurchenko, O., Melke, J., Fischer, A., Urban, G., *High electrocatalytic activity of metal-free and non-doped hierarchicalcarbon nanowalls towards oxygen reduction reaction.* Electrochimica Acta, 2018. **269**: p. 657-667.
49. Nicholson, R.S., *Theory and Application of Cyclic Voltammetry for Measurement of Electrode Reaction Kinetics.* Anal. Chem., 1965. **37**(11): p. 1351-1355.
50. Foster, C.W., J.P. Metters, and C.E. Banks, *Ultra Flexible Paper Based Electrochemical Sensors: Effect of Mechanical Contortion upon Electrochemical Performance.* Electroanalysis, 2013. **25**(10): p. 2275-2282.
51. Klingler, R.J., Kochi, J. K., *Electron-Transfer Kinetics from Cyclic Voltammetry. Quantitative Description of Electrochemical Reversibility.* J. Phys. Chem., 1981. **85**: p. 1731-1741.
52. Zhang, L.X., Sun, Z., Qi, J. L., Shi, J. M., Hao, T. D., Feng, J. C., *Understanding the growth mechanism of vertically aligned grapheneand control of its wettability.* Carbon, 2016. **103**: p. 339-345.
53. Zhao, R., Ahktar, M., Alruqi, A., Dharmasena, R., Jasinski, J. B., Thantirige, R. M., Sumanasekera, G. U., *Electrical transport properties of graphene nanowalls grown at low temperature using plasma enhanced chemical vapor deposition.* Mater. Res. Express, 2017. **4**: p. 055007.
54. Dresselhaus, M.S., Jorio, A., Hofmann, M., Dresselhaus, G., Saito, R., *Perspectives on Carbon Nanotubes and Graphene Raman Spectroscopy.* Nano Letters, 2010. **10**: p. 751–758.
55. Jorio, A., Dresselhaus, M. S., Saito, R., Dresselhaus, G., *Raman Spectroscopy in Graphene Related Systems*. 2011, Weinheim, Germany: Wiley-VCH Verlag GmbH & Co. KGaA.
56. Malard, L.M., Pimenta, M. A., Dresselhaus, G., Dresselhaus, M. S., *Raman spectroscopy in graphene.* PhysicsReports, 2009. **473**: p. 51-87.
57. Eckmann, A., Felten, A., Mishchenko, A., Britnell, L., Krupke, R., Novoselov, K. S., Casiraghi, C., *Probing the Nature of Defects in Graphene by Raman Spectroscopy.* Nano Letters, 2012. **12**: p. 3925−3930.
58. Ferrari, A.C., Robertson, J., *Interpretation of Raman spectra of disordered and amorphous carbon.* Physical Review B, 2000. **61**(20): p. 14095-14107.
59. Ferrari, A.C., Basko, D. M., *Raman spectroscopy as a versatile tool for studying the properties of graphene.* Nature Nanotechnology, 2013. **8**: p. 235-246.
60. Baranov, O., Levchenko, I., Xu, S., Lim, J. W. M., Cvelbar, U., Bazaka, K., , *Formation of vertically oriented graphenes: what are the key drivers of growth?* 2D Mater., 2018. **5**.
61. Ostrikov, K., Neyts, E. C., Meyyappan, M., *Plasma Nanoscience: from Nano-Solids in Plasmas to Nano-Plasmas in Solids.* Advances in Physics, 2013. **62**(2): p. 113-224.
62. Martins Ferreira, E.H., Moutinho, M. V. O., Stavale, F., Lucchese, M. M., Capaz, R. B., Achete, C. A., Jorio, A., *Evolution of the Raman spectra from single-, few-, and many-layer graphene with increasing disorder.* Phys. Rev. B, 2010. **82**.
63. McCreery, R.L., *Advanced Carbon Electrode Materials for Molecular Electrochemistry.* Chem. Rev., 2008. **108**: p. 2646–2687.
64. Streeter, I., Wildgoose, G. G., Shao, L., Compton, R. G., *Cyclic voltammetry on electrode surfaces covered with porouslayers: An analysis of electron transfer*

*kinetics atsingle-walled carbon nanotube modified electrodes.* Sensors and Actuators B: Chemical, 2008. **133**: p. 462–466.

65. Narula, U., Tan, C. M., *Qualitative Analysis of Growth Parameters for PECVD Based Low Temperature Synthesis of Graphene Using Design of Experiments.* Front. Mater., 2018. **5**(43): p. 1-7.
66. Guo, L., Zhang, Z., Sun, H., Dai, D., Cui, J., Li, M., Xu, Y., Xu, M., Du, Y., Jiang, N., Huang, F., Lin, C.-T, *Direct formation of wafer-scale single-layer graphenefilms on therough surface substrate by PECVD.* Carbon, 2018. **129**: p. 456-461.
67. Seo, D.H., Kumar, S., Ostrikov, K., *Control of morphology and electrical propertiesof self-organized graphenes in a plasma.* Carbon, 2011. **49**: p. 4331-4339.
68. Terasawa, T., Saiki, K., *Growth of graphene on Cu by plasma enhanced chemicalvapor deposition.* Carbon, 2012. **50**: p. 869-874.
69. Zhu, M., Wang, J., Holloway, B. C., Outlaw, R. A., Zhao, X., Hou, K., Shutthanandan, V., Manos, D. M., *A mechanism for carbon nanosheet formation.* Carbon, 2007. **45**: p. 2229-2234.
70. Brownson, D.A.C., Munro, L. J., Kampouris, D. K., Banks, C. E., *Electrochemistry of graphene: not such a beneficial electrode material?* RSC Advances, 2011. **1**: p. 978-988.
71. Ganguly, A., Sharma, S., Papakonstantinou,P. Hamilton, J., *Probing the Thermal Deoxygenation of Graphene Oxide Using High-Resolution In Situ X-ray-Based Spectroscopies.* J. Phys. Chem. C, 2011. **115**: p. 17009–17019.
72. Okpalugo, T.I.T., Papakonstantinou, P., Murphy, H., McLaughlin, J., Brown, N. M. D., *High resolution XPS characterization of chemical functionalised MWCNTs and SWCNTs.* Carbon, 2005. **43**: p. 153–161.